EUROPEAN ORGANIZATION FOR NUCLEAR RESEARCH (CERN)

CERN-EP-2022-199
2022/10/15

CMS-HIN-21-002

Azimuthal anisotropy of dijet events in PbPb collisions at $\sqrt{s_{\mathrm{NN}}} = 5.02\,\mathrm{TeV}$

The CMS Collaboration

Abstract

The path-length dependent parton energy loss within the dense partonic medium created in lead-lead collisions at a nucleon-nucleon center-of-mass energy of $\sqrt{s_{\mathrm{NN}}} = 5.02\,\mathrm{TeV}$ is studied by determining the azimuthal anisotropies for dijets with high transverse momentum. The data were collected by the CMS experiment in 2018 and correspond to an integrated luminosity of $1.69\,\mathrm{nb}^{-1}$. For events containing back-to-back jets, correlations in relative azimuthal angle and pseudorapidity (η) between jets and hadrons, and between two hadrons, are constructed. The anisotropies are expressed as the Fourier expansion coefficients v_n, $n = 2$–4 of these azimuthal distributions. The dijet v_n values are extracted from long-range ($1.5 < |\Delta\eta| < 2.5$) components of these correlations, which suppresses the background contributions from jet fragmentation processes. Positive dijet v_2 values are observed which increase from central to more peripheral events, while the v_3 and v_4 values are consistent with zero within experimental uncertainties.

Submitted to the Journal of High Energy Physics

1 Introduction

Hydrodynamic flow in relativistic heavy ion collisions is produced as initial-state geometry asymmetries transform into final-state momentum asymmetries. These asymmetries are commonly characterized by the Fourier expansion coefficients v_2, v_3, v_4, etc., of the particle azimuthal distributions. The anisotropic flow for hadrons in heavy ion collisions has been extensively studied at the BNL RHIC [1–14] and at the CERN LHC [15–29]. However, relatively few similar measurements have been done for jets [30–32]. Since partons fragmenting into high transverse momentum (p_{T}) jets are produced in hard processes, instead of emerging from the thermalized medium, they are not expected to "flow" in a hydrodynamic sense. However, the jet yields can exhibit correlations with the symmetry planes in an event since the evolving parton showers experience various in-medium path lengths or medium densities as they pass through the quark-gluon plasma [33–35]. In particular, the jets coplanar with the second-order symmetry plane, also known as the "event plane", are expected to suffer less energy loss, leading to a measurable v_2 signal. Indeed, azimuthal anisotropies of high p_{T} hadrons up to $\sim$100 GeV have been observed [24, 28], suggesting a path-length dependence of the parton energy loss. Performing dedicated jet azimuthal anisotropy measurements can greatly increase the accessible p_{T} range and give better estimates of the initial parton kinematics. The ATLAS and ALICE Collaborations have published inclusive jet v_2 results using data for lead-lead (PbPb) collisions at a nucleon-nucleon center-of-mass energy of $\sqrt{s_{\mathrm{NN}}} = 2.76$ TeV [30, 31]. The ATLAS collaboration subsequently extended this measurement to higher v_n harmonics at $\sqrt{s_{\mathrm{NN}}} = 5.02$ TeV [32]. The higher v_n harmonics for jets arise from fluctuations of initial state geometry or medium density. These studies find significant positive and centrality-dependent v_2 values for inclusive jets. The ATLAS study [32] also finds positive and mostly centrality-independent v_3 values for inclusive jets, while the v_4 coefficients are consistent with zero.

In this paper, we measure jet v_2, v_3, and v_4 coefficients in events containing back-to-back high-p_{T} jets, denoted as dijet v_n coefficients, via jet-hadron correlations. Data for lead-lead collisions at $\sqrt{s_{\mathrm{NN}}} = 5.02$ TeV with a total integrated luminosity of 1.69 nb^{-1} [36, 37] were collected by the CMS experiment in 2018. In contrast to previous jet v_n measurements that determine the inclusive jet v_n by the jet azimuthal correlation with the direction of maximum particle density [30–32], here the dijet v_n is determined from jet-hadron and hadron-hadron (hereafter referred to as "dihadron") correlations. The methodology developed for this work focuses on addressing the issue of nonflow contributions affecting the extracted harmonic coefficients. These nonflow correlations are a particular problem for high-energy jets for which, as a consequence of momentum conservation, there is a nearly back-to-back counterpart in azimuth. The "away-side" jet fragmentation products are known to significantly contribute to the flow-like correlations. For jet-hadron correlations, these contributions from jet fragmentation are addressed taking advantage of the properties of the dijet system, and for dihadron correlations they are mitigated with a hadron p_{T} cut. Then, a Fourier analysis is performed on large relative pseudorapidity $\Delta\eta$ ("long range") components of jet-hadron and dihadron correlations. To separate the jet and hadron v_n signals and extract the dijet v_n values, it is assumed that the measured jet-hadron and dihadron correlations factorize, i.e., they can be expressed as products of the jet and hadron v_n or the product of two hadron v_n values, respectively [22]. This work extends the suite of experimental methods and measurements that address details of the dependence of parton energy loss on in-medium path length and medium density fluctuations. Tabulated results are provided in the HEPData record for this analysis [38].

2 The CMS experiment

The central feature of the CMS apparatus is a superconducting solenoid of 6 m internal diameter, providing a magnetic field of 3.8 T. Within the solenoid volume are a silicon pixel and strip tracker, a lead tungstate crystal electromagnetic calorimeter, and a brass and scintillator hadron calorimeter, each composed of barrel and two endcap sections. Two hadron forward (HF) steel and quartz-fiber calorimeters complement the barrel and endcap detectors, extending the calorimeter from the range $|\eta| < 3.0$ provided by the barrel and endcap out to $|\eta| < 5.2$. The HF calorimeters are subdivided in azimuth (φ) into 20° modular wedges and further segmented to form 0.175×0.175 ($\Delta\eta \times \Delta\varphi$) "towers". The sum of the transverse energies detected in the HF detectors ($3.0 < |\eta| < 5.2$) is used to define the event centrality [39] in term of percentiles of the total inelastic hadronic cross section, with 0% corresponding to the largest overlap of the colliding nuclei.

The CMS silicon tracker measures charged-particle tracks within $|\eta| < 2.5$. It consists of 1856 silicon pixel and 15 148 silicon strip detector modules. Muons are measured in the range $|\eta| < 2.4$, with detection planes made using three technologies: drift tubes, cathode strip chambers, and resistive plate chambers.

Events of interest are selected using a two-tiered trigger system. The first level, composed of custom hardware processors, uses information from the calorimeters and muon detectors to select events at a rate of around 100 kHz [40]. The second level, known as the high-level trigger, consists of a farm of processors running a version of the full event reconstruction software optimized for fast processing, and reduces the event rate to around 1 kHz before data storage [41].

A detailed description of the CMS detector, together with a definition of the coordinate system used and the relevant kinematic variables, can be found in Ref. [42].

3 Event selection

The events are selected using a high-level trigger that requires at least one calorimeter-based jet with $p_{\mathrm{T}} > 100$ GeV. These jets are reconstructed using the anti-k_{T} jet clustering algorithm with a distance parameter of $R = 0.4$ [43]. The underlying event contribution is subtracted from the jets using an iterative method [44] before the jet p_{T} is compared to the threshold. A minimum bias triggered sample is also used in the analysis as a control sample. For the minimum bias trigger, we require that on each side of the interaction point there is at least one HF tower above the readout threshold in the range of ∼6–12 GeV [41].

To reduce contamination from beam-gas collisions, vertex and noise filters are applied following the example of previous analyses [45]. We require that there are at least three HF towers on each side of the detector with an energy deposit of at least 3 GeV per tower. The primary vertex is required to have at least two tracks and to be reconstructed within 15 cm of the nominal interaction point in the beam direction (z) and within 2 cm in the transverse direction. The shapes of the clusters in the pixel detector are required to be compatible with those expected in a PbPb collision at the vertex location. Finally, we require that there are no anomalous signal shapes or spatial distributions in the hadronic barrel and endcap calorimeter readout [46].

Simulated event samples are used in the analysis to correct for biases in the jet reconstruction resulting from the underlying flow modulation and to correct for jet resolution effects. These samples are produced by embedding hard jet events generated with the PYTHIA 8.226 event generator [47] with tune CP5 [48] in soft underlying events (i.e. particles created from the bulk medium) simulated with the HYDJET 1.9 event generator [49]. This is denoted as

the PYTHIA+HYDJET sample. The CMS detector response is simulated using the GEANT4 toolkit [50].

Because of the large number of elementary nucleon-nucleon collisions in central PbPb events, these events are more likely to produce jets compared to peripheral events with fewer collisions. To take this into account in the simulations, the charged-particle multiplicity distribution in the analysis region $|\eta| < 2.4$ for the PYTHIA+HYDJET simulation is weighted such that it matches the one in the data. An additional reweighting procedure is performed to match the position distribution of the primary vertices in the beam direction in simulation and data.

To identify high-p_T dijet events, the two jets with highest p_T in the range of $|\eta| < 2$ are located. The highest p_T jet is called the "leading jet" and is required to pass the p_T selection of $p_{T,1} > 120\,\text{GeV}$. The second-highest p_T jet is referred to as the "subleading jet" and is required to have $p_{T,2} > 50\,\text{GeV}$. The azimuthal angle φ between the leading and subleading jets is required to be $|\Delta\varphi_{1,2}| > 5\pi/6$, ensuring that the two jets are back-to-back. Finally, both jets are required to fall within $|\eta| < 1.3$ to ensure the most stable jet reconstruction performance and to allow for full tracker acceptance on both sides of the jets. The events containing such pairs of back-to-back jets are referred as "dijet events".

4 Jet and track reconstruction

For this study, jets are reconstructed using the anti-k_T algorithm with a distance parameter $R = 0.4$, as implemented in the FASTJET framework [51]. Only the calorimeter information is used as an input to the anti-k_T algorithm. The underlying event contribution is subtracted from the raw jet energy using an iterative "noise/pedestal" subtraction algorithm [44]. First, the mean energy $\langle E_T(\eta)\rangle$ and dispersion $\langle \sigma_T(\eta)\rangle$ for the calorimeter cells sharing the same η position is calculated. This determines the pedestal as a function of pseudorapidity $P(\eta) = \langle E_T(\eta)\rangle + \langle \sigma_T(\eta)\rangle$. Then, the pedestal values are subtracted from each calorimeter cell and jets are clustered from the pedestal-subtracted calorimeter towers using the anti-k_T algorithm with $R = 0.3$. In the next iteration step, the pedestal functions are calculated again, but this time excluding all towers that are within $R = 0.5$ of any reconstructed jet with $p_T > 15\,\text{GeV}$. The updated pedestal functions give the final estimate of the underlying event background. The background subtracted jet energy is further calibrated using jet energy corrections calculated as a function of p_T and η following the method described in Ref. [52].

We have chosen to reconstruct jets using only calorimeter information because this minimizes a reconstruction bias caused by the hydrodynamic flow. This bias arises from the use of the φ-averaged event energy in the underlying event subtraction. However, flow modulations lead to higher underlying event occupancies in the direction of the event plane compared to the direction perpendicular to it. This artificially enhances the v_2-like signal in jet-hadron correlations, since jets coplanar with the event plane have increased probability to pass the analysis selections. The same is true for higher order event planes, but with smaller effects. As calorimeters generally require higher p_T particles to produce a signal as compared to the tracker, and hydrodynamic flow is more strongly experienced by lower p_T particles, using only calorimeter information to reconstruct jets reduces the size of this bias significantly.

The track reconstruction used in PbPb collisions is described in Ref. [53]. The charged-particle tracks used in this analysis are required to have at least 11 hits in the tracker layers and satisfy a stringent fit quality requirement, where the fit χ^2, divided by the product of the number of fit degrees of freedom and the number of tracker layers hit, is required to be less than 0.18. To decrease the likelihood of counting nonprimary charged particles originating from secondary

decay products, it is required that the distance of closest approach of a charged-particle track to at least one primary vertex in the event divided by its uncertainty is less than 3. Furthermore, it is required that the relative p_{T} uncertainty for the tracks is less than 10%. Finally, in order to reduce the contribution of misreconstructed tracks with very high p_{T}, it is required that for tracks with $p_{\mathrm{T}} > 20\,\mathrm{GeV}$, there is an associated energy deposit in the calorimeters corresponding to at least half of the track momentum. Corrections for tracking efficiency, detector acceptance, and misreconstruction rate are obtained and applied following the procedures discussed in Ref. [45].

5 Jet-hadron and dihadron angular correlations

Correlations between jets and charged particles are studied using two-dimensional distributions of the relative pseudorapidity $\Delta\eta$ and relative azimuth $\Delta\varphi$ of the charged particles with respect to the jet axis. These distributions are constructed by correlating each charged particle with leading and subleading jets, separately, and are normalized by the number of dijets. The analysis uses three charged particle p_{T} ($p_{\mathrm{T}}^{\mathrm{ch}}$) bins with bin borders 0.7, 1, 2 and 3 GeV, and three centrality intervals, 0–10, 10–30, and 30–50%. Since the majority of the measured charged particles are hadrons, the charged particles are often referred to as hadrons in this paper.

The raw correlations give the per-dijet normalized yield of jet-hadron pairs from the same event

$$S^{\mathrm{raw}}(\Delta\eta, \Delta\varphi) = \frac{1}{N_{\mathrm{dijet}}} \frac{\mathrm{d}^2 N^{\mathrm{same}}}{\mathrm{d}\Delta\eta \mathrm{d}\Delta\varphi}, \tag{1}$$

where N_{dijet} is the number of dijets satisfying the selection criteria and N is the number of jet-hadron pairs. However, since the detector has limited acceptance in η, it is more likely to find jet-hadron pairs with small rather than large $\Delta\eta$ values. Thus, the raw correlation shapes have the charged-particle yield falling rapidly towards large $\Delta\eta$. Detector inefficiencies can also lead to nontrivial effects on the correlation distributions. A mixed-event method, where jets and hadrons from different events are paired, is used to correct for these effects [22, 54]. By construction, such mixed-event correlations have structures due to detector and acceptance effects, but contain no physics correlations. For the mixed events, we require the primary vertex positions along the beam axis to match within 0.5 cm and the centrality percentile to be within 0.5 percentage points of those for the original data events. The charged hadrons are selected from minimum bias events to minimize jet-induced bias and to adequately capture the long-range flow correlations of the underlying event. The mixed-event pair distribution is given by

$$ME(\Delta\eta, \Delta\varphi) = \frac{\mathrm{d}^2 N^{\mathrm{mixed}}}{\mathrm{d}\Delta\eta \mathrm{d}\Delta\varphi}. \tag{2}$$

The maximum of the mixed event distribution is found at $(0, 0)$ since no pairs with $\Delta\eta = 0$ and $\Delta\varphi = 0$ are lost as a consequence of finite acceptance. Thus, the ratio $ME(0,0)/ME(\Delta\eta, \Delta\varphi)$ gives the normalized correction factor. Then, we construct the per-dijet associated charged-particle yield, corrected for acceptance effects, as

$$S(\Delta\eta, \Delta\varphi) = \frac{1}{N_{\mathrm{dijet}}} \frac{\mathrm{d}^2 N}{\mathrm{d}\Delta\eta \mathrm{d}\Delta\varphi} = \frac{ME(0,0)}{ME(\Delta\eta, \Delta\varphi)} S^{\mathrm{raw}}(\Delta\eta, \Delta\varphi). \tag{3}$$

In order to study the v_n components for the dijets, we need to separate the short-range correlations from the long-range correlations in the acceptance-corrected distribution. The short-range correlations from jet fragmentation manifest themselves as a Gaussian-like peak around

$(\Delta\eta, \Delta\varphi) = (0, 0)$ together with an elongated peak in $\Delta\eta$ around $\Delta\varphi = \pi$. These are removed from the distribution by imposing selections in $\Delta\eta$ and $\Delta\varphi$ as illustrated in Fig. 1. First, we project the $\Delta\varphi$ distributions corresponding to the range $1.5 < |\Delta\eta| < 2.5$ from both leading and subleading jet-hadron distributions. For these projections, the short-range correlation contribution to the near-side ($|\Delta\varphi| < \pi/2$) distributions is negligible , but the elongated jet peak is still present in the away-side ($|\Delta\varphi| > \pi/2$) distribution. However, in a statistical distribution, the leading and subleading jet peaks are separated by $\Delta\varphi = \pi$. It follows that for an unbiased long-range $\Delta\varphi$ distribution LR, we can write $\mathrm{LR}(\Delta\varphi_{\mathrm{leading}}) = \mathrm{LR}(\pi - \Delta\varphi_{\mathrm{subleading}})$. As the near sides of the long-range leading and subleading jet-hadron distributions have negligible bias coming from the jet peak, the long-range $\Delta\varphi$ distribution in the entire 2π range can be found by combining the near sides of these two distributions and shifting the subleading one by π.

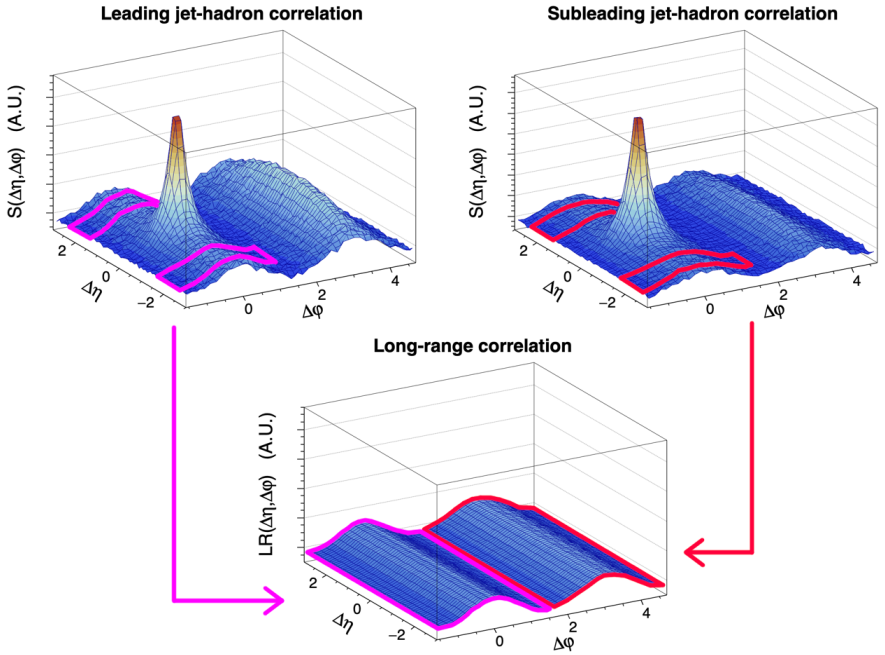

Figure 1: Illustration on how the long-range correlation distribution is constructed. The shape of the $\Delta\varphi$ projection corresponding to the range $1.5 < |\Delta\eta| < 2.5$ is determined from both leading and subleading jet-hadron correlation distributions for $|\Delta\varphi| < \pi/2$. The whole 2π range for the $\Delta\varphi$ distribution is obtained by combining these two components.

Once the long-range jet-hadron correlation distributions are projected on $\Delta\varphi$, the Fourier coefficients are found by fitting the distribution with the function

$$f_{\mathrm{Fourier}}(\Delta\varphi) = A\left(1 + \sum_{n=1}^{4} 2V_{n\Delta}\cos(n\Delta\varphi)\right), \tag{4}$$

where A is an overall normalization factor and $V_{n\Delta}$ is the fitted Fourier component of order n. When we fit the jet-hadron distribution, the extracted $V_{n\Delta}$ components reflect both the dijet and the hadron v_n values.

To obtain the hadron v_n values, we also construct dihadron correlations from the same dijet events as the jet-hadron correlations. We select all charged hadrons in the analysis hadron p_{T} bins as trigger particles, and pair them with all other charged particles in the same p_{T} bin, referred to as the associated particles. We follow the same event mixing procedure to correct for the detector and acceptance effects as for the jet-hadron correlations. However, since dihadron

correlations do not have jet information, the elongated jet peak cannot be removed from the away side of the correlation distribution. To mitigate the resulting background from high-p_{T} jet particles, we limit the hadron p_{T} selection with the highest $p_{\mathrm{T}}^{\mathrm{ch}}$ studied in the analysis to $2 < p_{\mathrm{T}}^{\mathrm{ch}} < 3\,\mathrm{GeV}$. One should notice that also for dihadron correlations, the dihadron $V_{n\Delta}$ values obtained from Eq. (4) are a mixture of trigger hadron v_n and associated hadron v_n values.

It is argued in Refs. [55, 56] that in the absence of nonflow correlations, the dihadron $V_{n\Delta}$ values factorize as

$$V_{n\Delta}^{\mathrm{dihadron}} = v_n^{\mathrm{trigger}} v_n^{\mathrm{associated}}, \tag{5}$$

where v_n^{trigger} is the v_n of the trigger hadron and $v_n^{\mathrm{associated}}$ is the v_n of the associated hadron. However, it is shown in Ref. [27] that p_{T} dependent event plane angle fluctuations can break the factorization, even without nonflow contributions. The validity of the factorization assumption is tested in Refs. [22, 57] and shown to work with good accuracy up to $p_{\mathrm{T}}^{\mathrm{associated}} \approx 4\,\mathrm{GeV}$. Above this p_{T} value, the factorization assumption starts to break down, primarily because of dijet fragmentation contributions. This is reflected in the upper hadron p_{T} limit in this analysis, as noted earlier. The jet-hadron correlation distributions are constructed in such a way that both the near- and the away-side dijet fragmentation contributions are explicitly removed. Thus, even though jets have very high p_{T} particles in them, the factorization is also expected to be a good approximation for the jet-hadron correlations.

Since the same momentum range for both trigger and associated hadrons is used for dihadron correlations, the hadron v_n can be extracted by taking the square root of the fitted dihadron $V_{n\Delta}$ values. By obtaining the hadron v_n in this way, we are able to calculate dijet v_n value using the factorization assumption:

$$v_n^{\mathrm{dijet}} = \frac{V_{n\Delta}^{\mathrm{jet\text{-}hadron}}}{v_n^{\mathrm{hadron}}}. \tag{6}$$

Each hadron p_{T} bin gives us a data point for the dijet v_n in the corresponding centrality bin. Since the dijet v_n should not depend on the hadron p_{T} selection used to extract it, we merge all three analysis hadron p_{T} bins to get the dijet v_n value from one wide $0.7 < p_{\mathrm{T}} < 3\,\mathrm{GeV}$ bin.

The dijet v_n values still need to be corrected for the jet reconstruction bias. This is done by determining the dijet v_n values from PYTHIA+HYDJET simulations where jets are embedded isotropically in the azimuthally anisotropic HYDJET background. The dijet v_n values extracted from this simulation study are, therefore, solely a result of the jet reconstruction bias.

The simulated events are tuned such that hadron v_2 and dihadron yields between data and simulation match, ensuring the most accurate correction possible. Both of these need to be matched simultaneously, since we need to correct for the absolute amount of energy that is added to or subtracted from the jets by the azimuthal anisotropies of the underlying event. Two different strategies are used to obtain this matching. For the nominal strategy, we start by matching the dihadron yields. This is achieved to a good accuracy by the multiplicity-based weighting that is applied to the PYTHIA+HYDJET simulation, as explained in Section 3. Then, we determine the hadron and dijet v_2 values from the simulation. An additional PYTHIA+HYDJET study showed that if the dihadron yield is kept constant and the hadron v_2 is varied by a certain percentage, the dijet v_2 value also changes by the same percentage. This means that we can get the proper dijet v_n corrections by determining the dijet v_n values from the simulation where only dihadron yields are matched, and scaling these values by the data-to-simulation hadron v_2 ratio. The jet reconstruction bias is then corrected by subtracting the v_n value obtained this way from the raw data dijet v_n value.

The second strategy used to evaluate systematic uncertainties matches the hadron v_2, and then applies a scaling factor to take into account the differences in dihadron yields. As a starting point for this strategy, we use a PYTHIA+HYDJET simulation, where instead of using the nominal multiplicity-based weighting to take into account the larger number of nucleon-nucleon collisions in central events, we use a centrality-based weighting scheme. In this scheme, we weight the centrality distribution determined from the HF calorimeters to match between data and simulation. Then, we check the underlying event energy density in random cones to see which centrality range in the simulation corresponds to similar energy densities in the data. The best match is found when the nominal centrality definition in the simulation is shifted 4 percentage points upwards. In this case, for example, the 0–10% centrality bin in data is matched with the 4–14% centrality bin in the PYTHIA+HYDJET simulation. After the centrality distributions are matched, we apply an event shape engineering method presented in Ref. [58] to match the hadron v_2 between simulation and data. It is shown in Ref. [58] that the elliptic flow and the magnitude of the second-order flow vector Q_2 normalized by the square root of event multiplicity are correlated. Thus, a selection based on this variable in the PYTHIA+HYDJET simulation event-by-event can be done to control the extracted hadron v_2 value. The Q_2-vector magnitude is defined as

$$Q_2 = \sqrt{Q_x^2 + Q_y^2}, \tag{7}$$

where

$$Q_x = \sum_i \cos(2\varphi_i),\ Q_y = \sum_i \sin(2\varphi_i). \tag{8}$$

Only particles from the HYDJET part of the simulation in $|\eta| < 0.75$ and $p_{\mathrm{T}} < 3\,\mathrm{GeV}$ are used. Using a Q_2-vector selection where hadron v_2 values in data and simulation match, the dijet v_n values are determined from the PYTHIA+HYDJET simulation. We have found in the previously described additional PYTHIA+HYDJET study that when hadron v_2 is kept the same, changing multiplicity does not affect the dijet v_2 linearly. Instead, we found a multiplicity-dependent function which allows us to calculate different scaling factors for each centrality bin. Thus, the dijet v_n values obtained after applying the Q_2-vector selection need to be scaled by the ratio of dihadron yields in data and simulation times this centrality dependent scaling factor. As before, the obtained dijet v_n values are subtracted from the raw data dijet v_n values to get the final corrected dijet v_n results.

6 Systematic uncertainties

The following sources of systematic uncertainty are considered in this analysis:

- *Acceptance correction*. Since jet correlations are small-angle correlations, and long-range correlations only depend on $\Delta\varphi$, the $\Delta\eta$ distribution at $|\eta| > 1.5$ should be uniform. To evaluate possible deviations from the uniformity that might arise from an imperfect acceptance correction, the analysis is repeated, extracting the long-range correlation distribution only from the negative ($-2.5 < \Delta\eta < -1.5$) or positive ($1.5 < \Delta\eta < 2.5$) sides of $\Delta\eta$. The larger difference from the nominal result is assigned as a systematic uncertainty.
- *Long-range extraction*. Uncertainties resulting from the long-range correlation distribution are determined by projecting the $\Delta\varphi$ distributions from two parts of the extraction region, $1.5 < |\Delta\eta| < 2.0$ and $2.0 < |\Delta\eta| < 2.5$. The larger difference from the nominal result is assigned as a systematic uncertainty.
- *Jet angular resolution*. The uncertainty in the jet angular resolution is estimated by determining the resolution in the PYTHIA+HYDJET simulation by comparing the

reconstructed- and generator-level jet axes. The jet axis in data is then allowed to vary by this amount and the results are compared with the nominal ones to determine the uncertainty.

- *Dijet bias in dihadron correlations*. It is possible that the dijet selection changes the hadron v_n with respect to minimum bias events. To check for this effect, we repeat the dihadron correlation measurement using a minimum bias data sample, and use the difference from the nominal results as an uncertainty.
- *Jet energy scale*. The related uncertainties are estimated by varying the jet energy corrections within their uncertainties and seeing how these changes affect the final correlations. The jet energy correction procedure is detailed in Ref. [52].
- *Jet energy resolution*. This uncertainty is estimated by comparing the nominal results with the ones obtained by adding a Gaussian spread to the nominal jet energies, as a function of jet p_{T}, such that the jet energy resolution estimated from the simulation is worsened by 20%. The value of 20% is determined by comparing dijet momentum balance $x_j = p_{\mathrm{T}}^{\mathrm{subleading}} / p_{\mathrm{T}}^{\mathrm{leading}}$ distributions in peripheral 50–70% and 70–90% bins between data and PYTHIA+HYDJET simulation. The jet energy resolution in the simulation is worsened by different amounts, and comparing the shapes of the resulting x_j distributions to data, it is seen that the maximal difference between jet energy resolutions in data and simulation is 20%.
- *Tracking efficiency*. The tracking-related uncertainties are estimated by repeating the analysis without any tracking corrections.
- *Jet reconstruction bias correction*. There are several sources of uncertainty related to the jet reconstruction bias correction. First, there is uncertainty on the dijet v_n values determined from the PYTHIA+HYDJET simulation. The dijet v_n values from the simulation in each centrality bin are extracted by performing a constant fit to the results from different hadron p_{T} bins up to $p_{\mathrm{T}}^{\mathrm{ch}} = 4\,\mathrm{GeV}$. The uncertainty of this fit is included in the uncertainty of the jet reconstruction bias correction.

  Second, we compare the dijet v_n results obtained using two different matching strategies between simulation and data to determine the correction. Both of these are described in detail in the end of Section 5.

  Third, the quark/gluon jet fraction in the PYTHIA+HYDJET simulation can be different from data, affecting the jet reconstruction bias correction. The potential difference is estimated to be less than 25% using a template fit to the multiplicity distribution of particle candidates within the jet cone in the data. Then, the uncertainty is estimated by varying the quark/gluon jet fraction in simulation by this amount. The particle candidates are leptons, photons, and charged and neutral hadrons that are reconstructed with a particle-flow algorithm [59] using an optimized combination of information from various elements of the CMS detector.

The total systematic uncertainties are obtained by adding all the individual components together in quadrature. The relative contributions from different sources are listed in Table 1 for the different dijet v_n harmonics. It can be seen from this table that the dominant source of uncertainty in most of the analysis bins arises from jet reconstruction. The jet reconstruction bias uncertainty is generally larger for higher v_n harmonics. While the simulated sample size is the same, the higher v_n coefficients have smaller signal sizes. Thus, they cannot be determined as accurately as the v_2 values for the correction.

Table 1: The breakdown of different sources of systematic uncertainty for dijet v_n, separately for the three centrality bins considered in the analysis.

v_n	Source	0–10%	10–30%	30–50%
v_2	Acceptance correction	0.002	<0.001	0.001
	Long-range extraction	0.003	0.003	0.002
	Jet angle resolution	<0.001	<0.001	0.001
	Jet reconstruction bias	0.008	0.003	0.006
	Dijet bias for dihadron	0.002	0.001	0.001
	Tracking	<0.001	0.001	<0.001
	Jet energy scale	0.002	0.001	0.002
	Jet energy resolution	0.004	0.003	0.002
	Total for v_2	0.010	0.005	0.007
v_3	Acceptance correction	<0.001	0.001	0.002
	Long-range extraction	0.002	0.001	0.006
	Jet angle resolution	0.001	0.001	0.001
	Jet reconstruction bias	0.005	0.016	0.016
	Dijet bias for dihadron	<0.001	0.001	0.001
	Tracking	<0.001	<0.001	0.001
	Jet energy scale	0.001	0.001	0.004
	Jet energy resolution	0.003	0.001	0.001
	Total for v_3	0.006	0.017	0.017
v_4	Acceptance correction	0.003	0.002	0.005
	Long-range extraction	0.003	0.003	0.001
	Jet angle resolution	0.001	<0.001	<0.001
	Jet reconstruction bias	0.018	0.016	0.026
	Dijet bias for dihadron	<0.001	<0.001	<0.001
	Tracking	<0.001	<0.001	0.002
	Jet energy scale	0.003	0.001	0.003
	Jet energy resolution	0.002	0.003	0.002
	Total for v_4	0.019	0.017	0.026

7 Results

The extracted dijet v_2, v_3, and v_4 values in different hadron p_T bins are presented in Fig. 2. All results shown in this figure are corrected for the jet reconstruction bias effects. Some dependence of the dijet v_n values on the reference particle p_T is observed, which is consistent with the expectation of possible factorization breaking by residual back-to-back correlations.

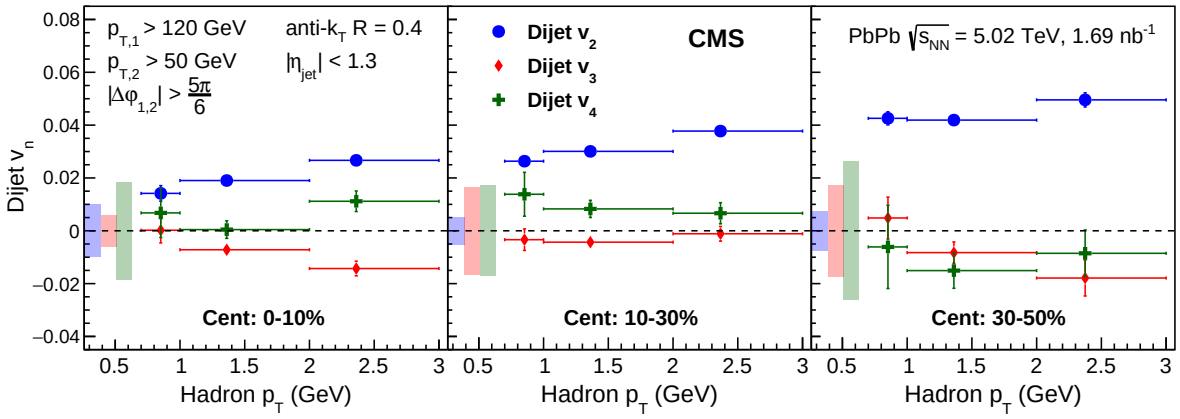

Figure 2: The dijet v_n data points factorized using different associated hadron p_T bins for 0–10% (left), 10–30% (middle), and 30–50% (right) centrality bins. The data points are corrected for the jet reconstruction bias effects. The vertical bars represent statistical uncertainties, while the p_T-independent systematic uncertainties are plotted as shaded areas on the left side of the panels.

The centrality dependence of the dijet v_n averaged over the reference particle p_T range of 0.7–3 GeV is presented in Fig. 3. The dijet v_2 measurements show positive values, indicating more jets observed coplanar with the event plane compared to the perpendicular direction. Since jets coplanar with event plane traverse less medium, these jets suffer less energy loss on average compared to those in the perpendicular direction. Thus, they are more likely to pass the analysis cuts, leading to the observed v_2 signal. The dijet v_2 magnitude is found to increase toward more peripheral collisions up to 30–50%, which is expected based on the increasing eccentricity of the collision overlap region. The current measurements are compared with previous CMS results on high-p_T hadron v_2 from Ref. [28]. Since that earlier work used finer centrality bins, the high-p_T hadron v_2 values plotted in Fig. 3 are compiled by first combining the centrality bins to match the ones used in this analysis, weighting each centrality bin by the number of events. Then, all hadron v_2 points above 20 GeV are fitted with a constant to define a value corresponding to contributions from the jet fragmentation. We observe that the measured dijet v_2 values are consistent with the high-p_T hadron v_2 values within the uncertainties, and similar values are also observed by the ATLAS collaboration in Ref. [32].

The dijet v_3 and v_4 results in the middle and right panels of Fig. 3 are found to be compatible with zero within experimental uncertainties in each centrality bin. These observations indicate that the fluctuations in the initial state geometry and medium density are insufficiently strong to produce a measurable impact on azimuthal distributions of dijets. The dijet v_3 results are also consistent with the CMS high-p_T hadron measurements in Ref. [28], which are also compatible with zero. In contrast, the recent ATLAS results show positive inclusive jet v_3 [32]. However, the ATLAS analysis is made with different selection criteria (lower jet p_T and smaller distance parameter) and the ATLAS inclusive jet and CMS dijet populations are different, so the two results should not be directly compared.

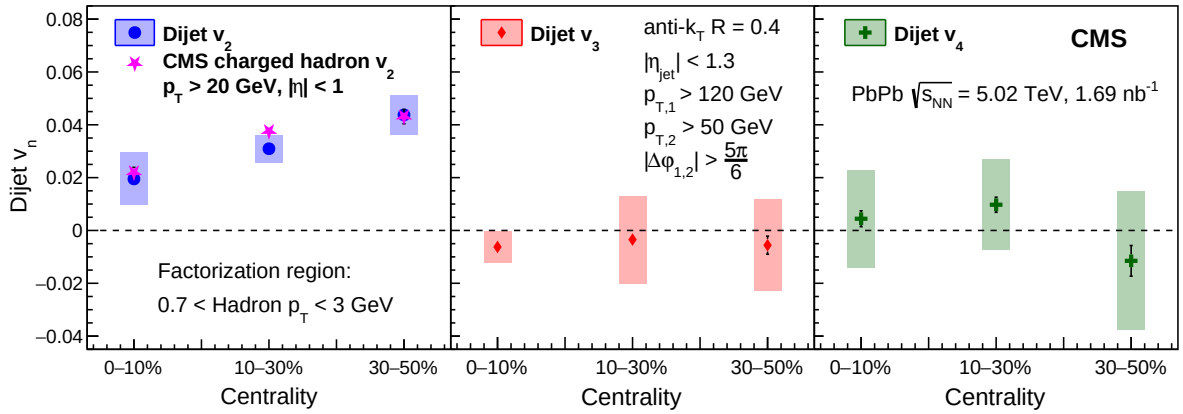

Figure 3: Final dijet v_2 (left), v_3 (middle), and v_4 (right) results presented as functions of centrality. The dijet v_2 results are compared to CMS high-p_T hadron v_2 results from Ref. [28]. The shaded areas represent systematic uncertainties and the vertical bars are the statistical uncertainties.

8 Summary

The Fourier coefficients v_2, v_3, and v_4 are determined for jets from events containing back-to-back jets ("dijet v_n") in lead-lead collisions at $\sqrt{s_{\mathrm{NN}}} = 5.02\,\mathrm{TeV}$. The jet-hadron correlation technique used for this measurement has been developed to unambiguously separate jet fragmentation-related contributions from the long-range correlations due to the in-medium path length and medium density dependencies of parton energy loss.

The dijet v_2 values are found to be positive, meaning that more jets are observed coplanar with the event plane than perpendicular to this plane. The dijet v_2 values increase with increasing eccentricity of the initial collision region, from about 2.0% in the 0–10% centrality bin to about 4.4% in the 30–50% centrality bin. These results are qualitatively consistent with expectations from a path-length dependence of in-medium energy loss. For all measured centrality bins, the dijet v_3 and v_4 values are consistent with zero within experimental uncertainties. Within the accuracy of this analysis, this shows that no significant modifications due to the initial state geometry and medium density fluctuations are seen in the jet azimuthal distributions. The measured dijet v_n values provide valuable input to a more precise and quantitative description of the partonic energy loss in the quark-gluon plasma.

References

[1] PHOBOS Collaboration, "Centrality and pseudorapidity dependence of elliptic flow for charged hadrons in Au+Au collisions at $\sqrt{s_{\mathrm{NN}}} = 200\,\mathrm{GeV}$", *Phys. Rev. C* **72** (2005) 051901, doi:10.1103/PhysRevC.72.051901, arXiv:nucl-ex/0407012.

[2] PHOBOS Collaboration, "System size, energy, pseudorapidity, and centrality dependence of elliptic flow", *Phys. Rev. Lett.* **98** (2007) 242302, doi:10.1103/PhysRevLett.98.242302, arXiv:nucl-ex/0610037.

[3] PHOBOS Collaboration, "Non-flow correlations and elliptic flow fluctuations in gold-gold collisions at $\sqrt{s_{\mathrm{NN}}} = 200\,\mathrm{GeV}$", *Phys. Rev. C* **81** (2010) 034915, doi:10.1103/PhysRevC.81.034915, arXiv:1002.0534.

[4] PHENIX Collaboration, "Elliptic flow of identified hadrons in Au+Au collisions at $\sqrt{s_{\rm NN}} = 200\,\text{GeV}$", *Phys. Rev. Lett.* **91** (2003) 182301, doi:10.1103/PhysRevLett.91.182301, arXiv:nucl-ex/0305013.

[5] PHENIX Collaboration, "Scaling properties of azimuthal anisotropy in Au+Au and Cu+Cu collisions at $\sqrt{s_{\rm NN}} = 200\,\text{GeV}$", *Phys. Rev. Lett.* **98** (2007) 162301, doi:10.1103/PhysRevLett.98.162301, arXiv:nucl-ex/0608033.

[6] PHENIX Collaboration, "Energy loss and flow of heavy quarks in Au+Au collisions at $\sqrt{s_{\rm NN}} = 200\,\text{GeV}$", *Phys. Rev. Lett.* **98** (2007) 172301, doi:10.1103/PhysRevLett.98.172301, arXiv:nucl-ex/0611018.

[7] PHENIX Collaboration, "Measurements of directed, elliptic, and triangular flow in Cu+Au collisions at $\sqrt{s_{\rm NN}} = 200\,\text{GeV}$", *Phys. Rev. C* **94** (2016) 054910, doi:10.1103/PhysRevC.94.054910, arXiv:1509.07784.

[8] PHENIX Collaboration, "Pseudorapidity dependence of particle production and elliptic flow in asymmetric nuclear collisions of p+Al, p+Au, d+Au, and ^{3}He+Au at $\sqrt{s_{\rm NN}} = 200\,\text{GeV}$", *Phys. Rev. Lett.* **121** (2018) 222301, doi:10.1103/PhysRevLett.121.222301, arXiv:1807.11928.

[9] STAR Collaboration, "Elliptic flow in Au+Au collisions at $\sqrt{s_{\rm NN}} = 130\,\text{GeV}$", *Phys. Rev. Lett.* **86** (2001) 402, doi:10.1103/PhysRevLett.86.402, arXiv:nucl-ex/0009011.

[10] STAR Collaboration, "Elliptic flow from two and four particle correlations in Au+Au collisions at $\sqrt{s_{\rm NN}} = 130\,\text{GeV}$", *Phys. Rev. C* **66** (2002) 034904, doi:10.1103/PhysRevC.66.034904, arXiv:nucl-ex/0206001.

[11] STAR Collaboration, "Particle type dependence of azimuthal anisotropy and nuclear modification of particle production in Au+Au collisions at $\sqrt{s_{\rm NN}} = 200\,\text{GeV}$", *Phys. Rev. Lett.* **92** (2004) 052302, doi:10.1103/PhysRevLett.92.052302, arXiv:nucl-ex/0306007.

[12] STAR Collaboration, "Azimuthal anisotropy in Au+Au collisions at $\sqrt{s_{\rm NN}} = 200\,\text{GeV}$", *Phys. Rev. C* **72** (2005) 014904, doi:10.1103/PhysRevC.72.014904, arXiv:nucl-ex/0409033.

[13] STAR Collaboration, "Elliptic flow of electrons from heavy-flavor hadron decays in Au+Au collisions at $\sqrt{s_{\rm NN}} = 200$, 62.4, and 39 GeV", *Phys. Rev. C* **95** (2017) 034907, doi:10.1103/PhysRevC.95.034907, arXiv:1405.6348.

[14] STAR Collaboration, "Measurement of D^0 azimuthal anisotropy at midrapidity in Au+Au collisions at $\sqrt{s_{\rm NN}} = 200\,\text{GeV}$", *Phys. Rev. Lett.* **118** (2017) 212301, doi:10.1103/PhysRevLett.118.212301, arXiv:1701.06060.

[15] ALICE Collaboration, "Elliptic flow of charged particles in Pb-Pb collisions at 2.76 TeV", *Phys. Rev. Lett.* **105** (2010) 252302, doi:10.1103/PhysRevLett.105.252302, arXiv:1011.3914.

[16] ALICE Collaboration, "Higher harmonic anisotropic flow measurements of charged particles in Pb-Pb collisions at $\sqrt{s_{\rm NN}} = 2.76\,\text{TeV}$", *Phys. Rev. Lett.* **107** (2011) 032301, doi:10.1103/PhysRevLett.107.032301, arXiv:1105.3865.

[17] ALICE Collaboration, "Elliptic flow of identified hadrons in Pb-Pb collisions at $\sqrt{s_{\rm NN}} = 2.76$ TeV", *JHEP* **06** (2015) 190, doi:10.1007/JHEP06(2015)190, arXiv:1405.4632.

[18] ALICE Collaboration, "Anisotropic flow of charged particles in Pb-Pb collisions at $\sqrt{s_{\rm NN}} = 5.02$ TeV", *Phys. Rev. Lett.* **116** (2016) 132302, doi:10.1103/PhysRevLett.116.132302, arXiv:1602.01119.

[19] ATLAS Collaboration, "Measurement of the pseudorapidity and transverse momentum dependence of the elliptic flow of charged particles in lead-lead collisions at $\sqrt{s_{\rm NN}} = 2.76$ TeV with the ATLAS detector", *Phys. Lett. B* **707** (2012) 330, doi:10.1016/j.physletb.2011.12.056, arXiv:1108.6018.

[20] ATLAS Collaboration, "Measurement of the azimuthal anisotropy for charged particle production in $\sqrt{s_{\rm NN}} = 2.76$ TeV lead-lead collisions with the ATLAS detector", *Phys. Rev. C* **86** (2012) 014907, doi:10.1103/PhysRevC.86.014907, arXiv:1203.3087.

[21] ATLAS Collaboration, "Measurement of the distributions of event-by-event flow harmonics in lead-lead collisions at $\sqrt{s_{\rm NN}} = 2.76$ TeV with the ATLAS detector at the LHC", *JHEP* **11** (2013) 183, doi:10.1007/JHEP11(2013)183, arXiv:1305.2942.

[22] CMS Collaboration, "Centrality dependence of dihadron correlations and azimuthal anisotropy harmonics in PbPb collisions at $\sqrt{s_{\rm NN}} = 2.76$ TeV", *Eur. Phys. J. C* **72** (2012) 10052, doi:10.1140/epjc/s10052-012-2012-3, arXiv:1201.3158.

[23] CMS Collaboration, "Measurement of the elliptic anisotropy of charged particles produced in PbPb collisions at $\sqrt{s_{\rm NN}} = 2.76$ TeV", *Phys. Rev. C* **87** (2013) 014902, doi:10.1103/PhysRevC.87.014902, arXiv:1204.1409.

[24] CMS Collaboration, "Azimuthal anisotropy of charged particles at high transverse momenta in PbPb collisions at $\sqrt{s_{\rm NN}} = 2.76$ TeV", *Phys. Rev. Lett.* **109** (2012) 022301, doi:10.1103/PhysRevLett.109.022301, arXiv:1204.1850.

[25] CMS Collaboration, "Measurement of higher-order harmonic azimuthal anisotropy in PbPb collisions at $\sqrt{s_{\rm NN}} = 2.76$ TeV", *Phys. Rev. C* **89** (2014) 044906, doi:10.1103/PhysRevC.89.044906, arXiv:1310.8651.

[26] CMS Collaboration, "Studies of azimuthal dihadron correlations in ultra-central PbPb collisions at $\sqrt{s_{\rm NN}} = 2.76$ TeV", *JHEP* **02** (2014) 088, doi:10.1007/JHEP02(2014)088, arXiv:1312.1845.

[27] CMS Collaboration, "Evidence for transverse momentum and pseudorapidity dependent event plane fluctuations in PbPb and pPb collisions", *Phys. Rev. C* **92** (2015) 034911, doi:10.1103/PhysRevC.92.034911, arXiv:1503.01692.

[28] CMS Collaboration, "Azimuthal anisotropy of charged particles with transverse momentum up to 100 GeV/c in PbPb collisions at $\sqrt{s_{\rm NN}} = 5.02$ TeV", *Phys. Lett. B* **776** (2018) 195, doi:10.1016/j.physletb.2017.11.041, arXiv:1702.00630.

[29] CMS Collaboration, "Principal-component analysis of two-particle azimuthal correlations in PbPb and pPb collisions at CMS", *Phys. Rev. C* **96** (2017) 064902, doi:10.1103/PhysRevC.96.064902, arXiv:1708.07113.

[30] ATLAS Collaboration, "Measurement of the azimuthal angle dependence of inclusive jet yields in Pb+Pb collisions at $\sqrt{s_{\mathrm{NN}}} = 2.76$ TeV with the ATLAS detector", *Phys. Rev. Lett.* **111** (2013) 152301, doi:10.1103/PhysRevLett.111.152301, arXiv:1306.6469.

[31] ALICE Collaboration, "Azimuthal anisotropy of charged jet production in $\sqrt{s_{\mathrm{NN}}} = 2.76$ TeV Pb-Pb collisions", *Phys. Lett. B* **753** (2016) 511, doi:10.1016/j.physletb.2015.12.047, arXiv:1509.07334.

[32] ATLAS Collaboration, "Measurements of azimuthal anisotropies of jet production in Pb+Pb collisions at $\sqrt{s_{\mathrm{NN}}} = 5.02$ TeV with the ATLAS detector", *Phys. Rev. C* **105** (2022) 064903, doi:10.1103/PhysRevC.105.064903, arXiv:2111.06606.

[33] X.-N. Wang, "Jet quenching and azimuthal anisotropy of large p_{T} spectra in noncentral high-energy heavy ion collisions", *Phys. Rev. C* **63** (2001) 054902, doi:10.1103/PhysRevC.63.054902, arXiv:nucl-th/0009019.

[34] M. Gyulassy, I. Vitev, and X.-N. Wang, "High p_{T} azimuthal asymmetry in noncentral A+A at RHIC", *Phys. Rev. Lett.* **86** (2001) 2537, doi:10.1103/PhysRevLett.86.2537, arXiv:nucl-th/0012092.

[35] E. V. Shuryak, "The azimuthal asymmetry at large p_{T} seem to be too large for a 'jet quenching"', *Phys. Rev. C* **66** (2002) 027902, doi:10.1103/PhysRevC.66.027902, arXiv:nucl-th/0112042.

[36] CMS Collaboration, "CMS luminosity measurement using nucleus-nucleus collisions at $\sqrt{s_{\mathrm{NN}}} = 5.02$ TeV in 2018", CMS Physics Analysis Summary CMS-PAS-LUM-18-001, 2022.

[37] CMS Collaboration, "Precision luminosity measurement in proton-proton collisions at $\sqrt{s} = 13$ TeV in 2015 and 2016 at CMS", *Eur. Phys. J. C* **81** (2021) 800, doi:10.1140/epjc/s10052-021-09538-2, arXiv:2104.01927.

[38] HEPData record for this analysis, 2022. doi:10.17182/hepdata.130961.

[39] CMS Collaboration, "Jet momentum dependence of jet quenching in PbPb collisions at $\sqrt{s_{\mathrm{NN}}} = 2.76$ TeV", *Phys. Lett. B* **712** (2012) 176, doi:10.1016/j.physletb.2012.04.058, arXiv:1202.5022.

[40] CMS Collaboration, "Performance of the CMS level-1 trigger in proton-proton collisions at $\sqrt{s} = 13$ TeV", *JINST* **15** (2020) P10017, doi:10.1088/1748-0221/15/10/P10017, arXiv:2006.10165.

[41] CMS Collaboration, "The CMS trigger system", *JINST* **12** (2017) P01020, doi:10.1088/1748-0221/12/01/P01020, arXiv:1609.02366.

[42] CMS Collaboration, "The CMS experiment at the CERN LHC", *JINST* **3** (2008) S08004, doi:10.1088/1748-0221/3/08/S08004.

[43] M. Cacciari, G. P. Salam, and G. Soyez, "The anti-k_{T} jet clustering algorithm", *JHEP* **04** (2008) 063, doi:10.1088/1126-6708/2008/04/063, arXiv:0802.1189.

[44] O. Kodolova, I. Vardanyan, A. Nikitenko, and A. Oulianov, "The performance of the jet identification and reconstruction in heavy ions collisions with CMS detector", *Eur. Phys. J. C* **50** (2007) 117, doi:10.1140/epjc/s10052-007-0223-9.

[45] CMS Collaboration, "Charged-particle nuclear modification factors in PbPb and pPb collisions at $\sqrt{s_{\mathrm{NN}}} = 5.02\,\mathrm{TeV}$", *JHEP* **04** (2017) 039, doi:10.1007/JHEP04(2017)039, arXiv:1611.01664.

[46] CMS Collaboration, "Identification and filtering of uncharacteristic noise in the CMS hadron calorimeter", *JINST* **5** (2010) T03014, doi:10.1088/1748-0221/5/03/T03014, arXiv:0911.4881.

[47] T. Sjöstrand et al., "An introduction to PYTHIA 8.2", *Comput. Phys. Commun.* **191** (2015) 159, doi:10.1016/j.cpc.2015.01.024, arXiv:1410.3012.

[48] CMS Collaboration, "Extraction and validation of a new set of CMS PYTHIA8 tunes from underlying-event measurements", *Eur. Phys. J. C* **80** (2020) 4, doi:10.1140/epjc/s10052-019-7499-4, arXiv:1903.12179.

[49] I. P. Lokhtin et al., "Heavy ion event generator HYDJET++ (HYDrodynamics plus JETs)", *Comput. Phys. Commun.* **180** (2009) 779, doi:10.1016/j.cpc.2008.11.015, arXiv:0809.2708.

[50] GEANT4 Collaboration, "GEANT4—a simulation toolkit", *Nucl. Instrum. Meth. A* **506** (2003) 250, doi:10.1016/S0168-9002(03)01368-8.

[51] M. Cacciari, G. P. Salam, and G. Soyez, "FastJet user manual", *Eur. Phys. J. C* **72** (2012) 1896, doi:10.1140/epjc/s10052-012-1896-2, arXiv:1111.6097.

[52] CMS Collaboration, "Jet energy scale and resolution in the CMS experiment in pp collisions at 8 TeV", *JINST* **12** (2017) P02014, doi:10.1088/1748-0221/12/02/P02014, arXiv:1607.03663.

[53] CMS Collaboration, "Description and performance of track and primary-vertex reconstruction with the CMS tracker", *JINST* **9** (2014) P10009, doi:10.1088/1748-0221/9/10/P10009, arXiv:1405.6569.

[54] CMS Collaboration, "In-medium modification of dijets in PbPb collisions at $\sqrt{s_{\mathrm{NN}}} = 5.02\,\mathrm{TeV}$", *JHEP* **05** (2021) 116, doi:10.1007/JHEP05(2021)116, arXiv:2101.04720.

[55] M. Luzum, "Collective flow and long-range correlations in relativistic heavy ion collisions", *Phys. Lett. B* **696** (2011) 499, doi:10.1016/j.physletb.2011.01.013, arXiv:1011.5773.

[56] B. H. Alver, C. Gombeaud, M. Luzum, and J.-Y. Ollitrault, "Triangular flow in hydrodynamics and transport theory", *Phys. Rev. C* **82** (2010) 034913, doi:10.1103/PhysRevC.82.034913, arXiv:1007.5469.

[57] ALICE Collaboration, "Harmonic decomposition of two-particle angular correlations in Pb-Pb collisions at $\sqrt{s_{\mathrm{NN}}} = 2.76\,\mathrm{TeV}$", *Phys. Lett. B* **708** (2012) 249, doi:10.1016/j.physletb.2012.01.060, arXiv:1109.2501.

[58] J. Schukraft, A. Timmins, and S. A. Voloshin, "Ultra-relativistic nuclear collisions: event shape engineering", *Phys. Lett. B* **719** (2013) 394, doi:10.1016/j.physletb.2013.01.045, arXiv:1208.4563.

[59] CMS Collaboration, "Particle-flow reconstruction and global event description with the CMS detector", *JINST* **12** (2017) P10003, doi:10.1088/1748-0221/12/10/P10003, arXiv:1706.04965.